Clays and Clay Minerals, Vol. 49, No. 2, 174–182, 2001.

HIGH-RESOLUTION TRANSMISSION ELECTRON MICROSCOPY STUDY OF NEWLY FORMED SEDIMENTS IN THE ATLANTIS II DEEP, RED SEA

NURIT TAITEL-GOLDMAN[1,2] AND ARIEH SINGER[2]

[1]The Open University, P.O. Box 39328 Tel-Aviv, Israel
[2]The Seagram Center for Soil and Water Sciences, Faculty of Agricultural, Food and Environmental Quality Sciences, The Hebrew University of Jerusalem, Rehovot, Israel

Abstract—Iron and silicon in various proportions are the major components of the newly formed hydrothermal sediments in the Atlantis II Deep, Red Sea. Iron-rich 2:1 phyllosilicates with morphologies varying from ribbons to plates represent clays in initial formation stage. Well-crystallized goethite particles contain domains of hundreds of nanometers in length with the rare presence of dislocations. Molar compositions show ratios of Si/Fe = 0.12 and Al/Fe = 0.05. Euhedral feroxyhyte with curled edges forms clusters with the goethite. The feroxyhyte has ratios of Si/Fe = 0.3 and are the major Si-associated iron oxides. Two nanometer-size phases showing short range periodity are common in the newly formed Atlantis II sediments: (1) hematite with traces of Si and (2) ferrihydrite with Si/Fe molar ratios varying between 0.17–0.89. The ferrihydrite forms large clusters. Hematite appears also as well-crystallized large crystals. Feroxyhyte probably forms at the transition zone between Red Sea Deep Water and the upper convective layer in the brine, whereas goethite and ferrihydrite form in the upper convective layer. The two forms of hematite represent two stages of recrystallization, which occur within the brine.

Key Words—Atlantis II Deep, Feroxyhyte, Ferrihydrite, Goethite, Hematite, HRTEM, Iron-Rich 2:1 Phyllosilicates.

INTRODUCTION

The Atlantis II Deep (A2D) is located in the actively diverging central part of the Red Sea. A submarine hydrothermal brine, which probably discharges into the South West (SW) basin, pools in the Deep to form denser layers of water than the overlying Red Sea Deep Water (RSDW). The hydrothermal brine is subdivided by sections of constant or nearly constant temperature: 55–56°C (upper convective layer-UCL2), 61–62°C (upper convective layer-UCL1), and 67.7°C (lower convective layer-LCL) (Hartmann *et al.*, 1998a, 1998b). Between the UCL2 and the RSDW lies the transition zone (TZ), which starts at 1980 m. The upper interface of the UCL2 is at 2008 m, the UCL1 surface is at 2020 m, and the LCL interface is at 2039 ± 5 m (Hartmann *et al.*, 1998a). Cl concentrations in these layers lie between 67 g of Cl per kg of water (67 g/kg) at the UCL2 to 158 g/kg in the LCL. The pH value decreases from 8.13 at RSDW to 5.2 at the LCL (Hartmann *et al.*, 1998a). The iron concentration in LCL reaches 75–81 mg/kg and is depleted in the UCL at 7 mg/kg (Hartmann, 1985).

The A2D has drawn scientific attention since its discovery. The sediments have been described by many (*e.g.*, Bischoff, 1969a, 1972; Bäcker and Richter, 1973; Cole, 1983, 1988; Badaut *et al.*, 1985; Singer and Stoffers, 1987; Schwertmann *et al.*, 1998). Clay minerals, iron oxides, carbonates, and sulfides are commonly found in the sediments, mainly in the upper part of the sedimentary column, whereas detrital minerals, sulfates, and pyrite along with clay minerals and iron oxides, comprise the lower column. Along with clay minerals, various phases of iron oxides and oxyhydroxides, *i.e.*, poorly crystalline goethite, hematite, lepidocrocite, ferrihydrite, and poorly crystalline hematite were identified in the sediments (Bischoff, 1969b; Pottorf, 1980; Knedler, 1985; Schwertmann *et al.*, 1998), whereas akaganeite and wüstite were detected in the overlying sampled brine (Holm *et al.*, 1982, 1983).

Hydrothermal plumes, which emerge along active diverging plate boundaries, such as the East Pacific Rise or the Mid Atlantic ridge, carry gas-rich fluids at elevated temperature (≤400°C) and of varying salinity (Von Damm, 1995). The association of Fe^{2+} and elevated Si concentrations in these plumes was described from many marine hydrothermal environments (Von Damm, 1995), *i.e.*, the Galapagos Spreading Center (McMurtry *et al.*, 1983) and seamounts in the East Pacific (Alt, 1988). Sulfides, silicates, and oxides crystallize and settle from discharging brine or precipitate and settle after mixing with deep ocean water. Iron-rich smectite, nontronite, is a common clay mineral in these environments. A pure Fe end member of the nontronite-beidelite series was described from the South Pacific (Singer *et al.*, 1984). Iron-rich smectites were found on seamounts in the eastern Pacific (Alt, 1988), on the Galapagos Spreading Center (McMurtry *et al.*, 1983), in the Bauer Deep (Cole and Shaw, 1983; Cole, 1985), and elsewhere along active hydrothermal sites. Feely *et al.* (1994) found that Fe-rich oxyhydroxides associated with silica occur at the north Clipperon Transform Fault and these phases are characteristic of a mature, high-temperature vent field.

The outstanding feature that is unique to the A2D from other submarine hydrothermal sites is that sedimentation and settling in the A2D occur within a dense, hot brine. Mixing of the brine discharge with RSDW is limited, leading to sedimentation and recrystallization in a hydrothermal environment of elevated salinity and temperatures.

Brewer and Spencer (1969) suggested that precipitation of crystalline iron oxyhydroxides occurs in the UCL, where Fe concentration is lower. The encounter between the iron diffusing up from the hydrothermal vent, with oxygen that is carried down by Mn^{4+} results in the formation of FeOOH precipitates, which sink to the bottom of the deep brine (Danielsson *et al.,* 1980).

The objective of this study was to identify and characterize authigenic, newly formed sediments, in initial formation state, that crystallized from the brine and were not subjected to any diagenetic processes. These sediments represent various crystallization environments in the A2D.

METHODS

Samples

Two samples studied were obtained from the SW basin of the A2D, Red Sea, at location no. 17022/2, 21°19.8′N, 38°05.012′E. The samples were collected during the SO121 expedition of the vessel RV Sonne in 1997. Water depth at this site is 2165 m. Sample GN255 was collected with a multi-corer from the top centimeter of a floppy sediment layer, whereas sample GN256 represents the suspension in the lowermost 10 cm of the overlying brine, above GN255. Sample GN255 was taken from the 10th tube of the multicorer. The moist samples were stored at 4°C in airtight boxes at collection on shipboard.

Methods and calculation. Each sample was kept under N_2 atmosphere while it was washed free of salts with distilled water from which dissolved oxygen was removed by bubbling N_2 gas. This method was used to prevent formation of iron oxides by oxidation of iron sulfides or iron carbonates which are common in sediments of A2D. The samples were then freeze-dried. X-ray diffraction (XRD) was performed on the dried samples. High-resolution transmission electron microscopy (HRTEM) was used for detailed study of the cryptocrystalline substances. For TEM analyses, powder from each sample was suspended in alcohol and placed on Cu-supported carbon films. The samples were analyzed using a Jeol 2010 HRTEM operated at 200 kv with an ISIS-system for energy dispersive analysis (Oxford Instrument Link). The beam width varied from 10 to 25 nm. The data obtained from the HRTEM were processed using fast Fourier transformation with Digital Micrograph (Gatan) software.

The calculation of the chemical formula of the 2:1 phyllosilicates was based on a unit cell with 44 negative charges and assuming that all iron was Fe^{3+}. For iron oxides, the molar Si/Fe ratio was calculated.

RESULTS

On the basis of morphology and chemical composition, particles were divided into detrital and authigenic phases. Clay minerals with aluminum content and quartz were considered detrital, and were probably derived from exposed crystalline or sedimentary rocks of the Red Sea. Pure Si-Fe phases (Si-associated iron oxides and Fe-rich clays), which reflect the composition of the discharging brine were considered authigenic.

Slightly rounded grains of quartz and clusters of clay minerals comprise the main detrital phases settling in the A2D. Kaolinite particles have hexagonal morphology but the corners are smoothed by transport, whereas 2:1 phyllosilicates form rounded clusters or thin sheets (Figure 1). The chemical, morphological, and structural characteristics of the detrital particles are given in Table 1.

Authigenic minerals derived form the brine consist of both amorphous and well-crystallized phases. Layered iron-rich silicates and Si-associated iron oxides were the main phases observed. Thus, iron and silicon in various proportions are the major components of the newly formed hydrothermal sediments.

Amorphous, xenomorphic silica, with no distinct electron diffraction pattern, forms thin layers (Figure 2). The amorphous silica occurs frequently associated with plates of 2:1 phyllosilicates. The chemical composition of the amorphous phase consists of silica only with no detected impurities. The morphology of this phase excludes a biogenic origin and suggests that the Si-O phase had precipitated either from the brine or at the brine-sediment interface.

Authigenic clays observed in the samples of A2D are mainly composed of 2:1 phyllosilicates on the basis of XRD and electron diffraction patterns. The tetrahedral occupancy is Si and the octahedra contain only iron and with no substitutions of other ions in either of the sheets. Most particles are thin and $\leq$10 nm wide. The clay particles have variable morphologies from very fine, sometimes curled sheets with vague outlines and without a clear morphology or very thin ribbons (Figure 3) to elongated plates with distinct edges (Figure 4). The chemical composition also varies, from Si/Fe = 0.4 to 2.4. The chemical, morphological, and *b* cell parameters calculated from *d*(060), are given in Table 2. The *b* parameters are close to nontronite (0.91 nm; Brindley, 1980).

Goethite particles occur as elongated individual needles or as composites of domains. Particle lengths of monodomain character are ~200 nm and widths are a few nanometers, whereas composite particles (multidomain) are much larger (Figure 5a). Each domain is 6–8 nm wide and is coherent with neighboring do-

Table 1. Chemical composition, morphology, and *d*(060) of detrital 2:1 clays in A2D.

Sample	Cation[1]	Tetrahedral[1]	Octahedral	Length (nm)	Width (nm)	*d*(060) (nm)[2]	Remarks
GN255	—	$Si_{7.29}Al_{0.71}$	$Al_{1.07}Fe_{1.4}Mg_{1.92}$	100	8	0.153	A cluster with curved layers
	$K_{0.88}$	$Si_{6.74}Al_{1.06}$	$Fe_{3.69}Mg_{0.93}$	420	150	0.151	Rounded cluster of particles
	$Ca_{1.65}$	$Si_{6.95}Al_{1.05}$	$Al_{2.3}Fe_{0.93}$	50	40	not measured	Plates
GN256	$K_{0.2}$	$Si_{7.76}Al_{0.24}$	$Al_{1.62}Fe_{1.89}Mg_{0.74}$	3200	1600	0.152	3 measurements in one particle
	$K_{0.3}$	$Si_{7.05}Al_{0.95}$	$Al_{0.236}Fe_{2.697}Mg_{0.96}$	3200	1600	0.152	
	$K_{0.26}$	Si_{8}	$Al_{1.88}Fe_{1.8}Mg_{0.36}$	3200	1600	0.152	
	$K_{0.25}$	$Si_{8.14}$	$Al_{2.23}Fe_{0.56}Mg_{1.38}$	160	100	not measured	One particle with unclear boundary
	—	$Si_{7.14}Al_{0.86}$	$Al_{0.68}Fe_{3.08}Mg_{0.79}$	5000–8000		0.152	Curved sheet
	$Ca_{0.15}$	$Si_{8.56}$	$Al_{1.33}Fe_{1.825}$			0.152	Curved sheet
		$Si_{7.14}Al_{0.86}$	$Al_{0.68}Fe_{3.08}Mg_{0.79}$				Curved sheet

[1] Calculation based on 44 negative charges, as obtained by analytical electron microscopy.
[b] Obtained by electron diffraction.

mains. Although dislocations are rare, the crystals are not perfect. HRTEM micrographs exhibit almost perfect crystallinity with spacing of (021) and (02$\bar{1}$) planes forming an angle of 115° (Figure 5b). HRTEM images were processed by fast Fourier transformation (FFT) to reduce the noise. This transformation yielded a lattice-image pattern from which *d*(021) values of 0.25 and 0.26 nm were obtained (Figure 5c). Dislocations occur in the calculated image, which lacks clarity owing to variations in crystal width.

HRTEM lattice fringes corresponding to (111) planes with spacing of 0.244 nm and fringes corresponding to (021) planes with spacings of 0.263 nm were observed in a twinned goethite crystal (Figure 6). Dislocations in this crystal are common, especially

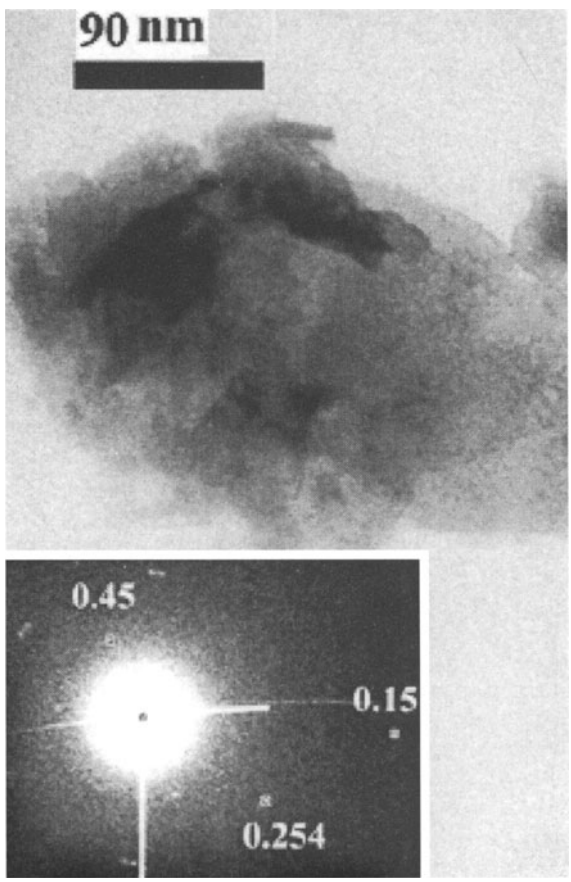

Figure 1. Detrital 2:1 phyllosilicate minerals in sample GN255.

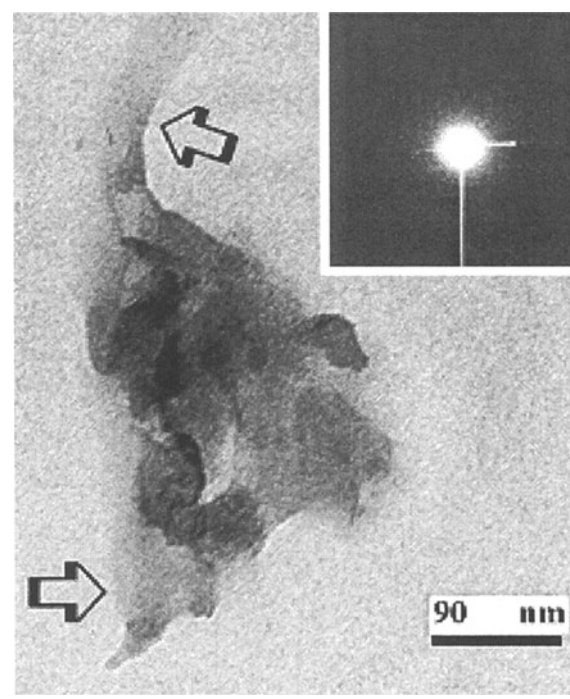

Figure 2. Amorphous silica (note arrows) in sample GN255, with some plates of 2:1 clay. Electron diffraction of amorphous silica in inset.

https://doi.org/10.1346/CCMN.2001.0490207 Published online by Cambridge University Press

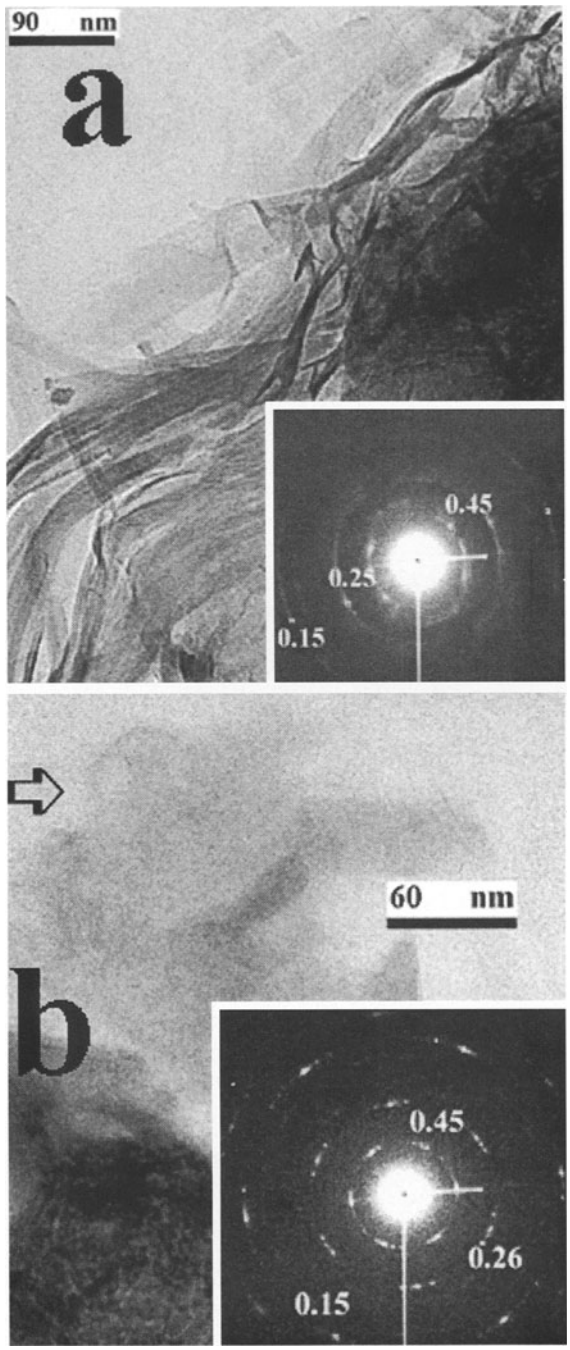

Figure 3. a) Curled authigenic 2:1 iron-rich clay mineral in sample GN255 with its electron diffraction pattern; b) authigenic iron-rich 2:1 phyllosilicate in sample GN255 (arrow points to the clay) and its electron diffraction pattern.

close to the incoherent twin boundary (arrow in Figure 6). The chemical composition of several goethite particles shows that mainly Si and traces of Al are associated with the goethite. The molar ratios are Si/Fe = 0.098–0.142 and Al/Fe = 0.046–0.058 (Table 3).

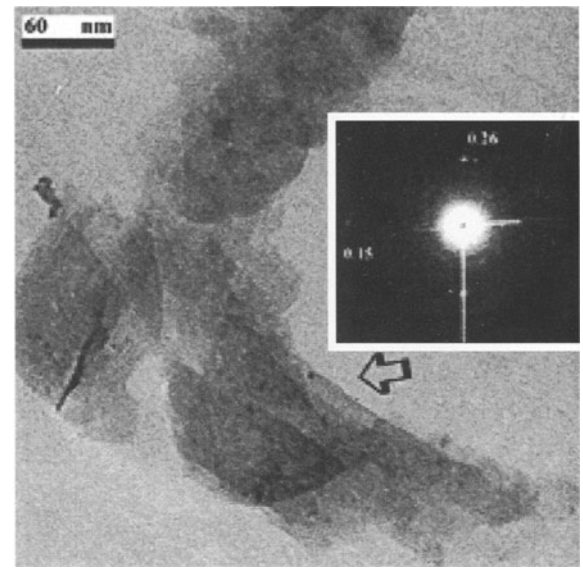

Figure 4. Platy authigenic 2:1 iron-rich phyllosilicate (arrow) in sample GN255 and its electron diffraction pattern.

Euhedral thin plates of feroxyhyte occur in both samples, with sizes to a few hundred nanometers. Rolling of the plates is common and they commonly occur in clusters (Figure 7a). Electron diffraction (0.252, 0.224, 0.144 nm) confirmed the identification as feroxyhyte (Figure 7b). Lattice images obtained on a curled edge of a particle exhibited two superposed plates of 4–5 nm width. (Figure 7c). No dislocations were observed. Chemical analyses obtained for feroxyhyte particles in GN255 and GN256 yielded Si/Fe = 0.30 and 0.41, respectively (Table 3).

Two-line ferrihydrite ($Fe_5HO_8 \cdot 4H_2O$) commonly appears in this sediment as 200-nm clusters composed of 4–5-nm size crystals (Figure 8a) with electron diffraction patterns showing d values of 0.256 and 0.145 nm (Figure 8b). The crystals are rounded and exhibit lattice-image domains with a spacing of 0.25–0.26 nm (Figure 8c). Numerical filtering by FFT of the lattice images indicated that the crystals are poorly crystalline, with curved lattice images caused by common dislocations (Figure 8d). Calculated diffraction patterns obtained with FFT suggest that the two-line ferrihydrite has hexagonal symmetry with spacings at 0.256 nm forming a grid with an angle of intersection of 100° (Figure 8e). Each two-line ferrihydrite particle examined is associated with varying amounts of Si, ranging between the composition of Si/Fe (molar ratio) of 0.17–0.89. The high Si concentration is probably related to imperfect crystallinity and the large surface area of the crystals.

Hematite subhedral crystals have perfect internal order (Figure 9a). Lattice images are shown in Figure 9b, and the FFT based on electron diffraction is presented in Figure 9c. Spacings are 0.25 and 0.24 nm,

https://doi.org/10.1346/CCMN.2001.0490207 Published online by Cambridge University Press

Table 2. Chemical composition, morphology, and $d(060)$ of authigenic 2:1 clays A2D.

Sample	Cation[1]	Tetrahedral[1]	Octahedral[1]	Length (nm)	Width (nm)	$d(060)$ (nm)[2]	Calculated b parameter	Remarks
GN255		$Si_{2.83}$	$Fe_{7.09}$	120	20	0.153	0.918	Very thin layer (2 chemical analyses)-Figure 3b
		$Si_{4.5}$	$Fe_{8.6}$					
		$Si_{8.54}$	$Fe_{3.33}$	400	30	0.15	0.9	Long, curled thin ribbons-Figure 3a
		$Si_{7.96}$	$Fe_{4.05}$	180	60	0.152	0.912	Plates-Figure 4
GN256		$Si_{9.98}$	$Fe_{1.35}$	250	—	0.150	0.9	Thin layer

[1] Calculation based on 44 negative charges, as obtained by analytical electron microscopy.
[2] Obtained by electron diffraction.

which form a perfect grid. The chemical composition of this crystal shows that it is nearly pure iron oxide with <5% Si content, which has no effect on the lattice image. Small, elongated crystals of hematite were observed with lattice fringe and diffraction spacings calculated at 0.37, 0.278, and 0.255 nm (Figure 10). Some crystals had platy morphology. These crystals are 5 nm wide and ~20 nm long. The platy crystals are 10 nm wide. The small size of the crystals and their dispersion on the grid caused a large error in the measured chemical composition, although the Si/Fe molar ratio is ~0.1. Despite the small size, some crystals exhibit perfect lattice image domains with no dislocations, indicating that Si content has no effect on the crystallinity.

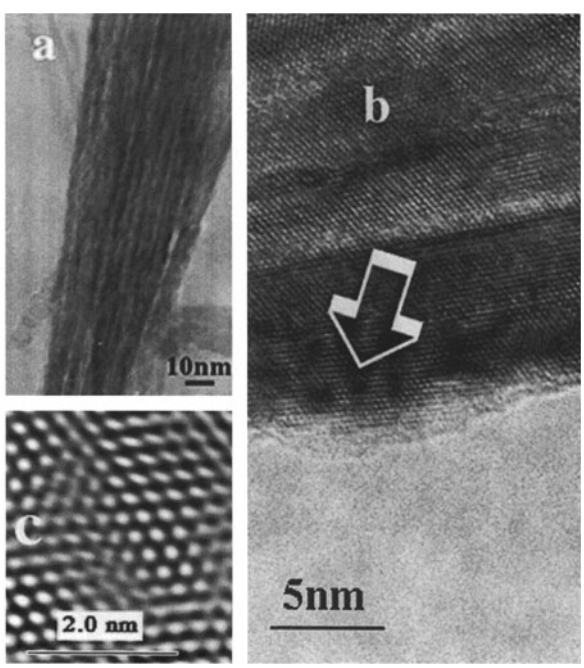

Figure 5. a) Multidomain particle of goethite in sample GN256; b) HRTEM micrograph of goethite crystal. (021) and (021) planes and the angle of 115° are shown. The arrow points at a dislocation; c) FFT of the goethite lattice image with some dislocations.

DISCUSSION

Amorphous silica, Fe-rich clays, and Si-associated iron oxyhydroxides, *i.e.*, goethite, feroxyhyte, ferrihydrite, and hematite, comprise the authigenic newly formed phases within the A2D brines. These brines differ in their physical and chemical properties.

The LCL is enriched with Si with respect to the underlying interstitial waters in the sediments and with respect to the overlying UCL1, UCL2, and RSDW. Because LCL is saturated with respect to SiO_2 (Anschutz and Blanc, 1995), amorphous silica precipitation may occur at this boundary layer or within the LCL, where the Si concentration remains constant.

According to Newman and Brown (1987), the term nontronite corresponds to dioctahedral smectite with octahedral $Fe^{3+} > 3$ per $O_{20}(OH)_4$. The chemical composition and the diffraction data indicate that the Fe-rich clays are probably nontronite. Iron-rich clay minerals, mainly nontronite, are found as major components in many hydrothermal marine environments such as in the mid-oceanic ridges or on submarine volcanic seamounts (McMurtry *et al.*, 1983; Singer *et al.*, 1984; Alt, 1988; Cole, 1985). The decrease in nontronite

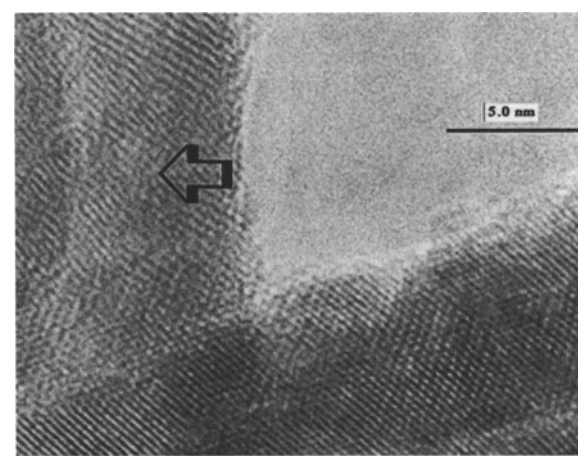

Figure 6. HRTEM micrograph of twinned goethite. Dislocations are common in the incoherent boundary and in the upper twin (arrow).

https://doi.org/10.1346/CCMN.2001.0490207 Published online by Cambridge University Press

Table 3. Chemical composition of iron oxides.

Iron oxide	Si/Fe[1]	Al/Fe[1]
Goethite	0.098–0.142	0.046–0.058
Feroxyhyte	0.3–0.41	—
Ferrihydrite	0.17–0.89	—
Hematite	0.1	—

[1] Obtained by analytical electron microscopy.

with increasing distance from the hydrothermal sites found in these studies suggests that nontronite crystallization is associated with hydrothermal activity. Nontronite and iron-rich smectite are found as common minerals in the sedimentary column of the A2D hydrothermally active site (Bischoff, 1969a, 1972). The uppermost facies throughout the A2D contains large amounts of iron-rich montmorillonite which is probably intermediate in composition between nontronite and a trioctahedral ferrous smectite (Bischoff, 1972).

In the A2D, Cole (1983, 1988) described authigenic nontronites and iron-bearing saponite, which differ in their oxygen-isotope formation temperature and Fe/Mg ratio. Cole concluded that the oxic nontronite from the carbonate-oxidic (CO) zone in A2D sediments was formed at 80°C, whereas the anoxic nontronite from the upper amorphous silicate zone (AM) facies was formed at higher temperatures (90–140°C). Cole proposed that the reciprocal-oxygen isotope temperature is linearly correlated with ln (Fe/Mg) in the octahedral sheet of authigenic nontronite. Decarreau *et al.* (1990), on the other hand, claimed that nontronite from the uppermost part of the sediments, crystallized at a lower temperature (70°C) and probably formed at the lower interface brine/recent deposits in the deep.

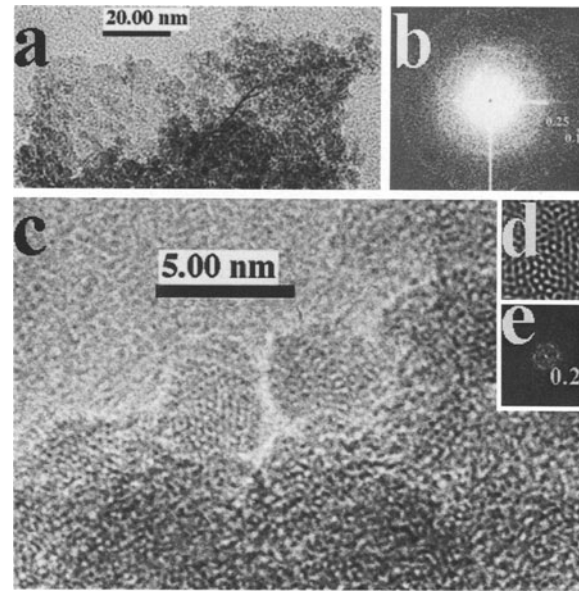

Figure 8. a) Cluster of ferrihydrite particles; b) Electron diffraction pattern of ferrihydrite cluster; c) Lattice-image domain of two-line ferrihydrite; d) FFT of two-line ferrihydrite showing lattice-image domain; e) Calculated electron diffraction of two-line ferrihydrite using FFT.

Because the nontronite-like phyllosilicates in our study were found both in the suspension and in the uppermost part of the sedimentary column, and by using the correlation of Cole (1988) between the Fe/Mg atomic ratio and the formation temperature, the formation temperature of these clays is probably not high, and they formed within the brine. Synthesis experiments of nontronite and Fe-rich smectite have shown that oxidation-reduction cycles are essential for crystallization (Harder, 1976, 1978; Decarreau and Bonnin, 1986; Decarreau *et al.*, 1987; Farmer *et al.*, 1994). Reducing and oxidizing cycles are possible within the

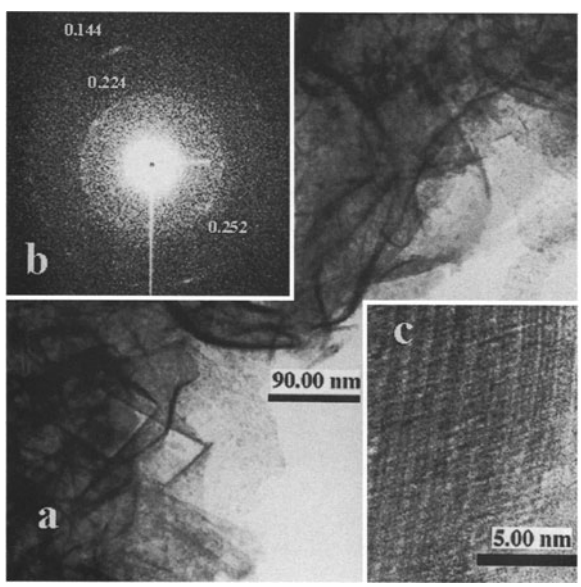

Figure 7. a) Feroxyhyte plates in sample GN255; b) Electron diffraction of the plates; c) Lattice image domain of feroxyhyte with no dislocations.

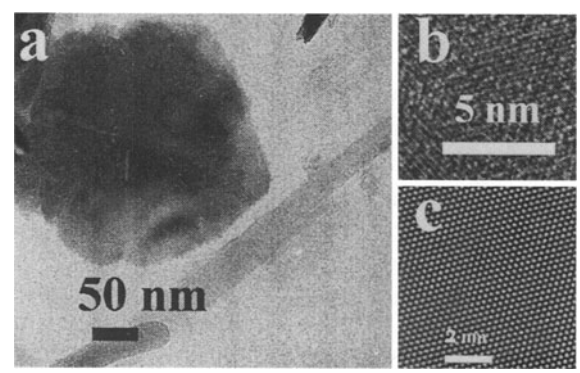

Figure 9. a) Subhedral large hematite crystal in sample GN256; b) HRTEM micrograph of hematite; c) FFT of the hematite.

https://doi.org/10.1346/CCMN.2001.0490207 Published online by Cambridge University Press

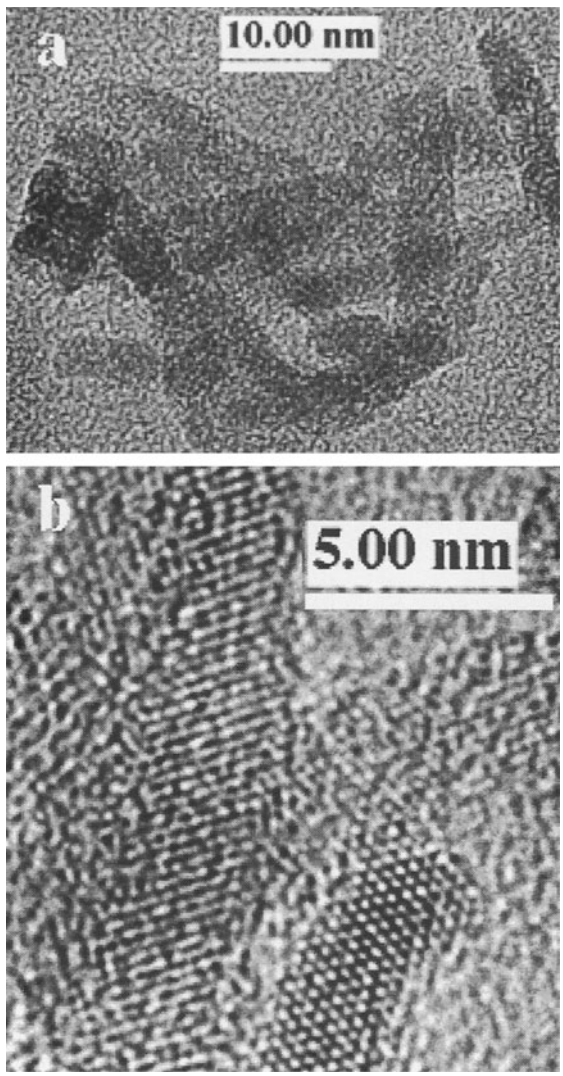

Figure 10. a) TEM micrograph of nano hematite crystals in sample GN256; b) HRTEM micrograph of nano hematite.

oxidized transition zone or at the UCL2 and UCL1, which are depleted in oxygen (Hartmann *et al.*, 1998a). These cycles are only possible if a venting mechanism is introduced into the brines to cause mixing and a temperature rise. We suggest that well-crystallized Fe-rich 2:1 clays were formed in UCL1 where the temperature is high and the Si concentration needed for their crystallization is greater. The less crystalline phases are probably formed in the UCL2 where less Si is available and the temperature is lower. Hartmann (1985) suggested that most of the iron precipitates at the LCL/UCL boundary and within the transition zone (TZ).

The multidomain character of goethite was attributed to crystallization from alkaline media (Cornell and Schwertmann, 1996). Thus, these large crystals were formed at the boundary between the brine, which supplies the iron needed, and the RSDW, where the concentration of oxygen and pH are higher. Large crystals are formed at lower Fe concentration where the number of nuclei is small. In contrast, small monodomain crystals of goethite probably formed in the UCL2 layer, still close to the high concentration of oxygen but at a lower pH and at higher temperature and Si concentration. Although the pH decreases downwards in the brine and goethite crystallization is enhanced under lower pH, it is unlikely that crystallization had occurred in the lower brine (LCL) because the concentration of oxygen is insufficient. Because the A2D brines have a composition that lies within the stability field of goethite and increasing pressure expands this stability field (Bischoff, 1969b), goethite probably crystallizes directly from the water without any precursor and not as a diagenetic product as suggested by Butuzova *et al.* (1990).

Feroxyhyte forms over a wide pH range, at extremely high oxidation conditions (Cornell and Schwertmann, 1996). Thus, crystallization of feroxyhyte, which is controlled by oxidation, probably occurs close to the TZ between RSDW and the uppermost brine layer. Formation in deeper layers, however, is not excluded.

Chukhrov *et al.* (1976) found feroxyhyte associated with Mn oxides in deep sea nodules. Because oxygen supply by Mn oxides was suggested as a mechanism for iron-oxide crystallization (Danielsson *et al.*, 1980), rapid dissolution of Mn oxides, which settle down from the RSDW into the brine, may have carried down the oxygen needed for crystallization. Chukhrov *et al.* (1977) noted that crystallization of feroxyhyte is possible at pH of 6–6.5, if silica is present. Crystallization at the UCL1 is thus possible, provided that the oxygen needed is supplied by the Mn oxides.

Ferrihydrite formation is favored by small amounts of silicate (Cornell and Schwertmann, 1996). Because SiO_2 concentrations are high in the brine, we suggest that goethite and ferrihydrite coprecipitate in the same layer depending on Si concentration. There was no evidence for microbiological precipitation of ferrihydrite as suggested by Butuzova *et al.* (1990).

Hematite crystallization is commonly attributed to a local temperature anomaly, suggesting close proximity to a zone of brine discharge (Bischoff, 1969b). Hematite usually forms from ferrihydrite by a solid-state reaction and involves dehydration and recrystallization. The latter is facilitated by the structural similarities between ferrihydrite and hematite (Cornell and Schwertmann, 1996). However, hematite found in the brine probably coprecipitated with ferrihydrite and was subjected to the same temperature as the ferrihydrite. Possibly, the transformation of ferrihydrite to hematite depends on Si concentration in the brine. At elevated Si concentrations, the transformation is retarded. The two sizes of hematite crystallites found in

the suspension may represent stages of transformation, with the smaller crystals not having reached the final stage of "maturation" as well-crystallized hematite. Knedler (1985) and Schwertmann *et al.* (1998) described poorly crystalline hematite in the upper part of a sedimentary column and well-crystallized hematite in the lower part. Because both phases coprecipitate in the brine, diagenesis within sediments is not the only mechanism allowing coexistence.

ACKNOWLEDGMENTS

The work was kindly supported by the authority of research in the Open University in Israel. We are grateful to P. Stoffers from the Christian Albrecht University, Kiel, Germany, for supplying the samples for this research. V. Ezerski, Ben-Gurion University, Israel, is thanked for HRTEM analyses. H. Stanjek, S. Guggenheim, and an anonymous reviewer are thanked for their enlightening and constructive remarks.

REFERENCES

Alt, J.C. (1988) Hydrothermal oxide and nontronite deposits on seamounts in the eastern Pacific. *Marine Geology,* **81,** 227–239.

Anschutz, P. and Blanc, G. (1995) Geochemical dynamics of the Atlantis II Deep. (Red Sea): Silica behavior. *Marine Geology,* **128,** 25–36.

Badaut, D., Besson, G., Decarreau, A., and Rauttureau, R. (1985) Occurrence of a ferrous, trioctahedral smectite in recent sediments of Atlantis II Deep, Red Sea. *Clay Minerals,* **20,** 389–404.

Bäcker, V.H. and Richter H. (1973) Die rezente hydrothermal-sedimentaire Lagerstatte Atlantis II Tief im Roten Meer. *Geologische Rundschau,* **62,** 697–741.

Bischoff, J.L. (1969a) Red Sea geothermal brine deposits, their mineralogy, chemistry and genesis. In *Hot Brines and Recent Heavy Metal Deposits in the Red Sea, Geochemical and Geophysical Account,* E.T. Degens and D.A. Ross, eds., Springer-Verlag, Berlin, 368–401.

Bischoff, J.L. (1969b) Goethite-hematite stability relations with relevance to sea water and Red Sea brine system. In *Hot Brines and Recent Heavy Metal Deposits in the Red Sea, Geochemical and Geophysical Account,* E.T. Degens and D.A. Ross, eds., Springer-Verlag, Berlin, 402–406.

Bischoff, J.L. (1972) A ferroan nontronite from the Red Sea geothermal system. *Clays and Clay Minerals,* **20,** 217–223.

Brewer, P.G. and Spencer, D.W. (1969) A note on the chemical composition of the Red Sea brines. In *Hot Brines and Recent Heavy Metal Deposits in the Red Sea, Geochemical and Geophysical Account,* E.T. Degens and D.A. Ross, eds., Springer-Verlag, Berlin, 174–179.

Brindley, G.W. (1980) Order-disorder in clay minerals structures. In *Crystal Structures of Clay Minerals and Their X-ray Identification,* G.W. Brindley and G. Brown, eds., Mineralogical Society Monograph No. 5, London, 125–195.

Butuzova, G.Yu., Drits, V.A., Morozov, A.A., and Gorschkov, A.I. (1990) Processes of formation of iron manganese oxyhydroxides in the Atlantis II and Thetis Deeps of the Red Sea. *Special Publications of the International Association of Sedimentology,* **11,** 57–72.

Chukhrov, F.V., Zvyagin, B.B, Gorshkov, A.I., and Sivtsov A.V. (1976) Mineralogical criteria in the origin of marine iron-manganese nodules. *Mineralium Deposita,* **11,** 24–32.

Chukhrov, F.V., Zvyagin, B.B., Gorshkov, A.I., Yermilova, L.P., Korovushkin, V.V., Rudnitskaya, Ye.S., and Yakubovskaya, N.Yu. (1977) Feroxyhyte, a new modification of FeOOH. *International Geological Review,* **19,** 873–890.

Cole, T.G. (1983) Oxygen isotope geochemistry and origin of smectites in the Atlantis II Deep, Red Sea. *Earth and Planetary Science Letters,* **66,** 166–176.

Cole, T.G. (1985) Composition, oxygen isotope geochemistry and origin of smectite in the metalliferous sediments of the Bauer Deep, southeast Pacific. *Geochimica et Cosmochimica Acta,* **49,** 221–235.

Cole, T.G. (1988) The nature and origin of smectite in the Atlantis II Deep, Red Sea. *Canadian Mineralogist,* **26,** 755–763.

Cole, T.G. and Shaw, H.F. (1983) The nature and origin of authigenic smectites in some recent marine sediments. *Clay Minerals,* **18,** 239–252.

Cornell, R.M. and Schwertmann, U. (1996) *The Iron Oxides, Structure, Properties, Reactions Occurrence and Uses.* VCH Weinheim, New York 573 pp.

Danielsson, L.G., Dyrssen, D., and Graneli, A. (1980) Chemical investigation of Atlantis II and Discovery brines in the Red Sea. *Geochimica et Cosmochimica Acta,* **44,** 2051–2065.

Decarreau, A. and Bonnin, D. (1986) Synthesis and crystallogenesis at low temperature of Fe(III)-smectite by evolution of coprecipitated gels: Experiments in partially reducing conditions. *Clay Minerals,* **21,** 861–877.

Decarreau, A., Bonnin, D., Badaut-Trauth, D., Couty, R., and Kaiser, P. (1987) Synthesis and crystallogenesis of ferric smectite by evolution of Si-Fe coprecipitates in oxidizing conditions. *Clay Minerals,* **22,** 207–223.

Decarreau, A., Badaut, D., and Blanc, G. (1990) Origin and temperature formation of Fe rich clays from Atlantis II Deep deposits (Red Sea). An oxygen isotopic geochemistry approach. *Geochemistry of Earth Surface and Mineral Formation, 2nd International Symposium, Aix en Provence France,* 363–364.

Farmer, V.C., McHardy, W.J., Elsass, F., and Robert, M. (1994) *hk*-ordering in aluminous nontronite and saponite synthesized near 90°C; Effects of synthesis conditions on nontronite composition and ordering. *Clays and Clay Minerals,* **42,** 180–186.

Feely, R.A., Gendron, J.F., Baker, E.T., and Lebon, G.T. (1994) Hydrothermal plumes along the East Pacific Rise, 8°40′ to 11°50′N: Particle distribution and composition. *Earth and Planetary Science Letters,* **128,** 19–36.

Harder, H. (1976) Nontronite synthesis at low temperature. *Chemical Geology,* **18,** 169–180.

Harder, H. (1978) Synthesis of iron layer silicate minerals under natural conditions. *Clays and Clay Minerals,* **26,** 65–72.

Hartmann, M. (1985) Atlantis II Deep geothermal brine system. Chemical processes between hydrothermal brines and Red Sea deep water. *Marine Geology,* **64,** 157–177.

Hartmann, M., Scholten, J.C., Stoffers, P., and Wehner, F. (1998a) Hydrographic structure of brine filled deeps in the Red Sea—new results from Shaban, Kerbit, Atlantis II and Discovery Deep. *Marine Geology,* **144,** 311–330.

Hartmann, M., Scholten, J.C., and Stoffers, P. (1998b) Hydrographic structure of brine filled deeps in the Red Sea: Correction of Atlantis II Deep temperatures. *Marine Geology,* **144,** 331–332.

Holm, N.G., Wadsten, T., and Dowler, M.J. (1982) β-FeOOH (akaganeite) in the Red Sea. *Estudios Geológicos,* **38,** 367–371.

Holm, N.G., Dowler, M.J., Wadsten, T., and Arrhenius, G. (1983) β-FeOOH·Cl_n (akaganeite) and $Fe_{1-x}O$ (wüstite) in hot brine from the Atlantis II Deep (Red Sea) and the uptake of amino acids by synthetic β-FeOOH·Cl_n. *Geochimica et Cosmochimica Acta,* **47,** 1463–1470.

Knedler, K.E. (1985) A geochemical and ^{57}Fe Mossbauer investigation of East Pacific Rise and the Red Sea metalliferous sediments and other selected marine sedimentary deposits, Ph.D. thesis, Victoria University of Wellington, New Zealand, 356 pp.

McMurtry, G.M., Wang, C.H., and Yeh, H.W. (1983) Chemical and isotopic investigation into the origin of clay minerals from the Galapagos hydrothermal mounds field. *Geochimica et Cosmochimica Acta,* **47,** 475–489.

Newman, A.C.D. and Brown, G. (1987) The chemical constitution of clays. In *Chemistry of Clays and Clay Minerals.* A.C.D. Newman, ed., Mineralogical Society Monograph No. 6, London, 1–110.

Pottorf, R.J. (1980) Hydrothermal sediments of the Red Sea, Atlantis. II Deep—a model for massive sulfide-type ore deposits. Ph.D. thesis, Pennsylvania State University, University Park, Pennsylvania, 193 pp.

Schwertmann, U., Friedl, J., Stanjek, H., Murad, E., and Bender Koch, C. (1998) Iron oxides and smectites in sediments from the Atlantis II Deep, Red Sea. *European Journal of Mineralogy,* **10,** 953–967.

Singer, A. and Stoffers, P. (1987) Mineralogy of a hydrothermal sequence in a core from the Atlantis II Deep, Red Sea. *Clay Minerals,* **22,** 251–267.

Singer, A., Stoffers, P., Heller-Kallai, L., and Szafranek, D. (1984) Nontronite in a deep sea core from the South Pacific. *Clays and Clay Minerals,* **32,** 375–383.

Von Damm, K.L. (1995) Controls on the chemistry and temporal variability of seafloor hydrothermal fluids. In *Seafloor Hydrothermal Systems: Physical, Chemical Biological and Geological Interactions, Geophysical Monograph 91,* S.E. Humphris, R.A. Zierenberg, L.S. Mullineaux, and R.E. Thomson, eds., The American Geophysical Union, 222–247.

E-mail of corresponding author: nuritg@oumail.openu.ac.il
(*Received 19 January 2000; accepted 13 November 2000; Ms. 423; A.E. Helge Stanjek*)